RESEARCH ARTICLE

Synthesis, Impedance and Current-Voltage Spectroscopic Characterization of Novel Gadolinium Titanate Nano Structures

Vinayak M Adimule[1,*], Debdas Bhowmik[2], Adarsha Haramballi Jagadeesha[3]

[1]VTU Recognized Research Centre of Chemistry, Department of Chemistry, Angadi Institute of Technology and Management (AITM), Savagaon Road, Belagavi 5800321, Karnataka, India
[2]High Energy Materials Research Laboratory, Défense Research and Development Organization, Ministry of Defence, Government of India, Sutarwadi, Pune 411021, India
[3]Centre for Research in Medical Devices, National University of Ireland, Gaillimh, Galway- H91TK33, Ireland

*Corresponding author: E-mail: adimulevinayak@yahoo.in; Tel.: (+91) 9481268717

DOI: 10.5185/amlett.2021.061638

Gadolinium (Gd) doped titanate nanostructures (NS) with a new set of 10-50 wt. % of Gd were synthesized by microwave-assisted hydrothermal and reduction using hydrazine hydrate. The crystal structure has been evaluated with SEM (scanning electron microscopy) analysis exhibited rod like geometry of nanoparticles (NPs). XRD (X-ray diffraction spectroscopy) analysis of $GdTiO_3$ and undoped titanate nanostructure (NS) intense peak exhibited crystal tetragonal structure. CV (cyclic voltammetry) exhibited an oxidation potential of 50 wt. % of $GdTiO_3$ was found to be - 0.54 eV. UV-Visible spectroscopic revealed absorptivity of 50 wt. % of $GdTiO_3$ was found to be 650 nm (visible region) and undoped titanate absorptivity at 320 nm (UV region). The pelletized nanostructures of $GdTiO_3$ were investigated for current-voltage (I-V), capacitance-voltage (C-V), resistance-voltage (R-V) measurements, which showed frequency range in between 1 kHz to 2 MHz and 50 wt. % $GdTiO_3$ NS showed a decreasing trend in admittance value with an increase in frequency. However, an increase in the conductance, power dissipation values with a decrease in resistivity, and increase in the frequency has been noticed which embark considerable variation in conductivity and power dissipation in $GdTiO_3$ NS. The results from the plots of current-voltage (I-V), capacitance-voltage (C-V), and bias voltage with an applied frequency of the $GdTiO_3$ NS has been discussed.

Introduction

In recent years nanomaterials synthesized by various methods have been studied for their unique attractive electrical and electronic properties like current-voltage [**1**], capacitance-voltage [**2**], LED [**3**] (light-emitting diodes), biosensor [**4**], gas sensor [**5**], impedance [**6**] and PCE [**7**] (power conversion efficiency), etc. Amongst rare-earth doped nanomaterials finds exceptional uses as compared to other nanostructures (NS). The distinctive features of tetragonal geometry of the titanium dioxide NS and their existence as branched and tetragonal shaped structures were reported in the literature [**8,9**]. Studies related to current-voltage (I-V) properties involve investigations of impedance, admittance, power dissipation, and other related quantity as a function of applied frequency and bias voltage. Rare earth metal NS significantly studied in catalytic reactions, high-performance luminescence devices, and other functional NS because of their unique optical, electronic, and chemical properties [**10**]. Rare earth titanate NS exhibits interesting dielectric, piezoelectric, and ferroelectric properties as reported in the literature [**11–13**]. However, Gd possesses a half-filled 4f-shell and an empty 5d shell which imparts unique electronic configuration and stability to $GdTiO_3$ NS [**14**]. Nanostructures of pure $SrTiO_3$, Sr_{1-x} Gd_xTiO_3 (Gd, $0 < x < 0.09$), and $Sr_{1-x}Gd_xTi_{1-y}NbyO_3$ with high cubic structure exhibited high power factor depending on the size of cubes [**15**]. Gd doped cobalt ferrites (Co Fe_{2-x} Gd_xO_4) with variable Gd (x = 0.0 to 0.4) content synthesized by solid-state ceramic method and studied for impedance spectroscopic analysis over a wide range of temperature and frequency. Incorporation of Gd^{+3} ions into Co ferrites induced structural disorder, lattice strains which have profound influence on the electrical conductivity and impedance properties of the NS [**16**]. Nanostructured $(Pb_{1-x}Sr_x)$ TiO_3 thin films prepared by chemical solution deposition processes [**17,18**] exhibits size-dependent dielectric properties at higher frequency and investigated their temperature-dependent I-V characteristics, leakage current and impedance of the thin films. Impedance spectroscopy (IS) and its applications related to electronic properties of nanomaterials discussed in detail by Nikolaos Bonanos *et. al.*, [**19**]. A L Alexe-Ionescu *et. al.*, [**20**] discussed in detail I-V characteristics of electrolytic cells, ohmic conduction, adsorbing-desorbing mechanism and theoretical approach to study role of impedance on the I-V curves. Graphene/SiO_2 based FET fabricated on metallic bilayer electrodes showed electrical properties, transport properties evidencing

significant reduction in carrier mobility and increase in the contact time [**21**]. Richard Galos *et. al.*, [**22**] studied sensor performance of PZT nano fibres, electrical impedance and I-V characteristics of NS. Applications of NPs in electrical impedance tomography [**23**] for the detection of tumours in presence of sensitizer, conductivity of the NPs inside tumours widely studied. Polymer doped $BaTiO_3$ hybrid NPs were studied I-V, C-V, their electrical bistability mechanism [**24**] in polymer memory devices. Epitaxial ferroelectric lead zirconate titanate showed transition of local electronic transport in NS between low and high bias regimes [**25**] the spatial variations due to heterogeneity of the interfacial electronic barrier and random changes in the tip contact geometry of the NPs. The 5 wt. % Y doped PbS NS prepared by precipitation chemical synthesis route showed the higher values of dielectric loss (37.8–178.6), dielectric constant (23.6–28.0), and electrical conductivity of the order of [10.2 to (11.7) S/m] at the lower frequency [**26**]. $ZnTiO_3$ nanopowders [**27**] investigated for their I-V, C-V and photovoltaic dye-sensitized solar cell performance, studies revealed differences in electrical properties and morphological features of NS. The Sm and Nb incapacitated 90% of $BaTiO_3$-10% of $Li_{0.5}Fe_{2.5}O_4$ nanocomposites reported conductivity peak of 90BLF nanocomposites lifted towards higher frequency with rise in concentration of Sm and Nb [**28**]. Titanate nanotubes synthesized by hydrothermal method investigated for their non-linear I-V behaviour, effects of bias voltage, exhibited an increase in bias voltage due to a decrease in dielectric constant and electrode capacitance [**29**]. Md. T. Rahman [**30**] *et. al.*, reported the Gadolinium (Gd) substituted cobalt ferrites ($CoFe_{2-x}Gd_xO_4$, referred to the CFGO) with variable Gd content (x = 0.0–0.4) have been synthesized by solid state ceramic method and showed electrical properties of Gd incorporated Co ferrite ceramics are enhanced compared to pure $CoFe_2O_4$ due to the lattice distortion. Mohd Shkir *et. al.*, [**31**] studied the dielectric constant was noticed in range of 25 to 57 of strontium (Sr) doped Lead Sulfide (PbS) (PbS:Sr) nanoparticles and the enhancement in total electrical conductivity was observed from -11.67 to -7.83 S/cm at 10 kHz; and from -4.30 to 3.42 S/cm at 10MHz. From the above evidence, in the present research work, author reported the effect of doping 10-50 wt. % Gd to the titanate NS, synthesized by microwave-assisted hydrothermal method followed by reduction using hydrazine hydrate. Morphology, crystal structure, optical properties, and I-V characteristics of $GdTiO_3$ NS were described. In particular pelletized $GdTiO_3$ NS were experimentally studied for their I-V, C-V, bias voltage properties by varying applied frequency and possible potential applications of $GdTiO_3$ NS investigated in detail.

Experimental

Materials and methods

Synthetic raw materials were purchased from e-Merck, Sigma Aldrich, Spectrochem Ltd., and used without any purification. Scanning electron and ion microscope (SEM) from ZEISS international high-resolution EVO family embedded EDS solution used for identification of crystal morphology of NS. Crystal structure of the synthesized $GdTiO_3$ investigated by X-ray diffraction instrument with HyPix-3000 high energy resolution from Rigaku smart lab having D/teX Ultra 250 silicon strip detectors. Optical properties were recorded using specord 210 plus analytic jean with variable spectral resolution and cooled double beam detection was incorporated for UV-Visible absorption spectrum. CH instruments Inc model 600E series used for the electrochemical measurements with scan rate in cyclic voltammetry (CV) 1000 V/s with a 0.1 mV potential increment. Samples were prepared pellets by using a hydraulic press machine and pressure of 1000 psi applied for 1-2 minutes. The thickness of the pellets maintained ~ 200 µm to ~ 400 µm and for establishing contacts silver paste (front and back end) was used over the surface of thin pellet. Properties of the NS changes slightly upon pelletizing samples and current-voltage, impedance, conductance, power dissipation was investigated by using Agilent 4294 instrument with variable series of frequencies ranging from 40 Hz to 110 MHz and applied DC voltage varies in between - 40V to + 40V.

Materials and methods

Synthesis of $GdTiO_3$ Nanostructures

Step 1: Synthesis of Gadolinium Oxide (Gd_2O_3) NS

$Gd(NO_3)_3.6H_2O$ (99.8 % purity from Sigma Aldrich) added with distilled water, placed in a magnetic stirrer, stirred for 1-2 h at room temperature, NH_4OH solution was added drop wise till pH = 11, subsequently obtained $Gd(OH)_3$ precipitate was filtered, dried at 100-200 °C, calcinated at 750-800 °C and obtained as amorphous off white Gd_2O_3 solid powder.

Reactions:

$$Gd(NO_3)_3 \xrightarrow{NH_4OH} Gd(OH)_3 + 3NO_2 \quad (1)$$

$$2Gd(OH)_3 \longrightarrow Gd_2O_3 + H_2O \quad (2)$$

Step 2: Doping Gd_2O_3 to titanate nanostructures

Gadolinium Oxide (10 wt. %, 20 wt. % and 50 wt. %) containing Gd^{+3} ions in the crystal and $TiCl_4$ were dissolved in deionized water (5-10 ml), transferred to microwave reaction vessel (2.45 GHz, 3 bar, 140-150 °C and 1000W) irradiated with microwave for 20 minutes (5 minutes/interval) in presence of surface reducing agent hydrazine hydrate monohydrate (2-5 drops) after completion of the reaction white precipitate was filtered, washed with cold water, ethanol-water and dried at 100-200 °C, calcinated at 700-800 °C, yielded white coloured $GdTiO_3$ NS.

Reactions:

$$TiCl_4 + 2H_2O \longrightarrow TiO_2 + 4HCl \quad (3)$$

$$2Gd_2O_3 + 2TiO_2 \xrightarrow{2H_2O/N_2H_4} 4GdTiO_3 + 2H_2(g) + N_2(g) \quad (4)$$

Results and discussion

Cyclic Voltammetry Investigation (CV)

The formation of best negative electrodes of $GdTiO_3$ NS, their electrochemical performance of the different wt. % of $GdTiO_3$ was carried out by cyclic voltammetry. CV characteristics of $GdTiO_3$ NS were evaluated with scan rate of 5 mV/second, applied potential varied between 0-2 V. Width of the CV curves decreases [**32,33**] in the order of undoped titanate < 20 wt. % $GdTiO_3$ < 40 wt. % $GdTiO_3$ < 50 wt. % $GdTiO_3$ demonstrating the reduction in case of undoped titanate NS **Fig. 1(a)** as compared with 50 wt. % $GdTiO_3$ NS **Fig. 1(b)**. The oxidation potential of the undoped titanate NS **Fig. 1(a)** was found to be - 0.11 eV and for 50 wt. % $GdTiO_3$ was found to be - 0.54 eV respectively. Electro activity of the NPs increased due to the incorporation of Gd^{+3} ions into titanate NS.

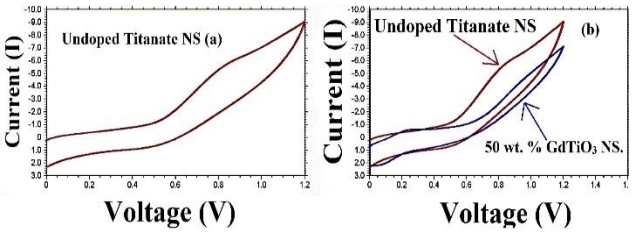

Fig. 1. (a) Electrochemical CV spectrum of undoped titanate (b) 50 wt. % $GdTiO_3$ nanostructures.

XRD studies

The X-ray diffractometer spectral patterns investigated for the undoped titanate (**Fig. 2(a)**), 10 wt. % $GdTiO_3$ (**Fig. 2(b)**) and 50 wt. % of $GdTiO_3$ (Figure 2(c)) respectively. X-ray photons absorbed at 2θ values ranging from 20 to 80 degrees. Intense diffraction peak was evaluated for determination of lattice parameters, grain size, grain boundary of the NPs of $GdTiO_3$. Crystallinity [**34-35**] of titanate decreases after the introduction of Gd^{+3} ions and also decreases the crystallite size. Incorporation of Gd^{+3} ions restricts the grain boundary movement and limits the growth of the crystals. Gd doping decreases the crystal size due to the formation of Gd-O-Ti bond over the surface of dopant NS which hinders the growth of crystal grains. When ionic radii of the dopant ion (Gd^{+3}, 0.938 A°) greater than the host ion ($Ti^{+4,}$ 0.569 A°) interplanar distance (d) and peak intensity shifts XRD patterns towards a higher angle. A decrease in the interplanar distance results in contraction of the lattice due to the creation of vacancy sites. Lattice contraction imparts electrostatic interaction of the dopant cations (Gd^{+3}) which results in stearic effect in NS. Average crystallite size of undoped titanate is in the range of 33.21 nm to 83.01 nm whereas 50 wt. % $GdTiO_3$ is in between 21.11 nm to 73.31 nm. **Table 1** shows (D) value, FWHM (full width half maximum), lattice parameters, peak positions (h k l), Bragg's angle (2θ) and angle shift (Δ2θ) of undoped titanate, 10 wt. % $GdTiO_3$ and 50 wt. % $GdTiO_3$ NS. Lattice (h k l) planes compared with (ASTM JCPDS file no. 23-0259) corresponds to the composition of $Gd_2Ti_2O_7$ NS. Zhanshen Zheng *et. al.*, [**36**] reported the dense microstructure of the samples doped with 0.5 mol % Gd^{+3} ions which indicates the addition of Gd^{+3}/Gd_2O_3 can promote grain growth over titanate NS. Crystallographic phase identification revealed Gd^{+3} ions well incorporated into titanate NS. The size of the crystallites of $GdTiO_3$ is calculated from XRD data using the Scherer's formula D (hkl) = k λ/β cos θ, where, λ is the wavelength (Cu, Kά) of X-ray, β is FWHM, θ is diffraction angle, D is crystallite size. It is evident that the crystallinity, size, phase composition of the rare earth NS solely dependent on the synthetic routes. It can be concluded that interplanar distance decreases after doping Gd^{+3} ions which is evident from the D values (**Table 1**).

Table 1: Peak positions, [h k l] planes, Braggs angle (2θ), Lattice parameters, Crystallite size (D) of undoped titanate, 10 wt. % $GdTiO_3$ and 50 wt. % $GdTiO_3$ NS.

Samples	[h k l]	Braggs Angle 2θ (°)	Angle Shift Δ2θ (°)	Lattice Parameters	FWHM (°)	Crystallite Size (D) (nm)
Undoped titanate	[111]	26.2	-	a = 3.74, b= 4.17	0.215 ± 0.014	63.41
	[200]	30.1	-	a = 4.05, b= 5.47	0.285 ± 0.011	43.52
	[220]	46.2	-	a = 7.11, b= 5.01	0.347 ± 0.075	43.68
	[311]	55.0	-	a = 6.12, b= 4.57	0.398 ± 0.013	53.57
	[400]	65.4	-	a = 5.22, b= 5.57	0.356 ± 0.015	33.21
	[331]	70.2	-	a = 6.78, b= 5.41	0.417 ± 0.010	83.01
10 wt. % $GdTiO_3$	[111]	28.9	2.7	a = 4.74	0.215 ± 0.010	43.21
	[200]	32.2	2.1	a = 5.21, b= 5.78	0.201 ± 0.097	52.81
	[220]	46.8	0.6	a = 3.89, b= 4.05	0.412 ± 0.096	31.71
	[311]	55.8	0.8	a = 3.98, b= 6.74	0.337 ± 0.002	24.51
	[400]	67.1	1.7	a = 4.52, b= 4.37	0.325 ± 0.057	33.61
	[331]	71.2	1.0	a = 4.11, b= 4.85	0.347 ± 0.064	53.41
50 wt. % $GdTiO_3$	[101]	26.4	-	a = 7.10, b= 5.11	0.210 ± 0.017	73.31
	[102]	27.8	-	a = 4.98, b= 4.52	0.305 ± 0.017	60.11
	[006]	31.9	-	a = 3.52	0.372 ± 0.011	53.71
	[110]	45.9	-	a = 3.14, b= 5.17	0.364 ± 0.005	51.51
	[220]	50.1	3.9	a = 5.74	0.357 ± 0.008	21.11
	[116]	56.4	-	a = 8.84, b= 2.58	0.387 ± 0.017	38.51
	[208]	70.2	-	a = 7.52, b= 2.64	0.470 ± 0.009	37.61

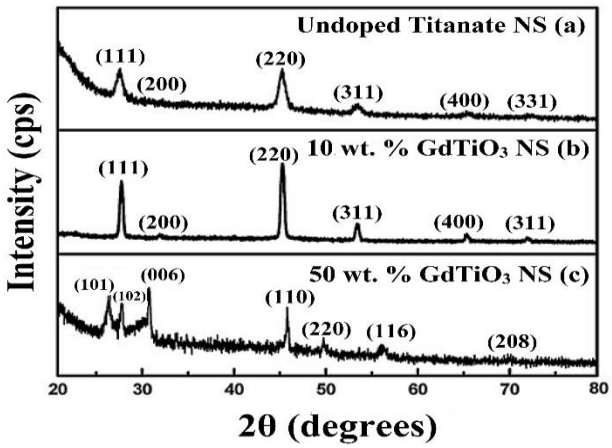

Fig. 2. (a) XRD patterns of the undoped titanate (b) 10 wt. % $GdTiO_3$ and (c) 50 wt. % of $GdTiO_3$ NS.

Scanning Electron Microscopy (SEM) studies

The Scanning electron microscopic experiments were performed for powder sample of $GdTiO_3$ to understand the grain size, grain boundary, interpore distance and overall distribution of the dispersed NPs. $GdTiO_3$ NS with average size (~ 50 nm) of Gd^{+3} ions distributed homogeneously over the titanate NS. However, undoped titanate NPs (**Fig. 3(a)**) showed tetragonal geometry with little agglomeration in the crystal structure [**37**]. Insertion of Gd^{+3} ions into the titanate NS increases the density of the crystal and more agglomeration was observed as the wt. % of impurity Gd^{+3} increases (**Figs. 3(b), 3(c)** and **3(d)**). This phenomenon is ascribed as the nucleation of Gd^{+3} assisted by oxygen groups present over titanate NS. Moreover, the content of Gd^{+3} ions increasing on the surface of titanate causes an increase in the density of the overall $GdTiO_3$ NS. Wenshuo Kang *et. al.*, [**38**] reported dense microstructures of the samples doped with 0.5 mol % Gd^{+3} ions without interconnected porosity, exhibits addition of Gd_2O_3 can promote overall grain growth of NPs. From the top view of the undoped and 50 wt. % $GdTiO_3$ NS showed tetragonal crystal structure and particle agglomeration. The average grain size, interpore distance, and average grain boundary of undoped titanate was found to be ~ 55 nm, ~ 80 nm, ~110 nm whereas for 50 wt. % $GdTiO_3$ NS was ~ 60 nm, ~ 70 nm, ~ 100 nm respectively. Close examination of the 10 wt. % of $GdTiO_3$ NS revealed porosity, cracks, and small holes after calcination at 800 °C. Average grain size, interpore distance and grain boundary was found to be ~ 51 nm, ~74 nm and ~ 111 nm. On the other hand, 20 wt. % $GdTiO_3$ NS has similar morphological structure with cavities formed on the surface due to solid-solid diffusion. Grain size, interpore distance and grain boundary was found to be ~ 54 nm, ~ 71 nm and ~ 96 nm respectively. Similar behaviour was realized when Gd doped to Mn_3O_4 NS calcinated at 700 °C. Architecture becomes thread bundle rod-like NS with particle agglomeration. The formed holes were on the surface of NS due to CO and CO_2 gas evolved during calcination. SEM images also reveal that the particle size is a distinct rod-like structure as the Gd^{+3} ion concentration increases agglomeration of NPs. Average grain size, grain boundary distance was ~ 62 nm and ~ 101 nm. Significant voids are created when the size of the dopant (Gd^{+3} ions) increases due to Kirkendall effect [**39**].

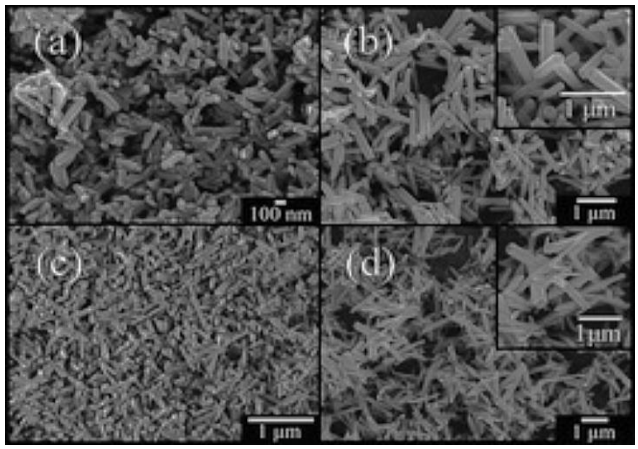

Fig. 3. (a) SEM morphological images of undoped titanate (b) 10 wt. % of $GdTiO_3$ and (c) 20 wt. % $GdTiO_3$ (d) 50 wt. % of $GdTiO_3$ NS.

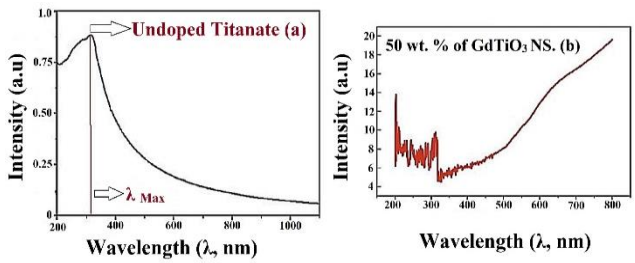

Fig. 4. (a) Optical absorption spectrum (UV-Visible) of undoped titanate (b) 50 wt.% $GdTiO_3$ nanostructures.

UV-Visible Spectroscopic Investigation

The Optical properties of $GdTiO_3$ NS were studied by using UV-Visible spectroscopic investigation (**Fig. 4**). Absorptivity was recorded for undoped titanate NS (**Fig. 4(a)**) and 50 wt. % $GdTiO_3$ (**Fig. 4(b)**). Wavelength of the spectrophotometer is limited to 800 nm and the blue shift in the spectrum after 500 nm is due to the presence of a polarized surface area of the $GdTiO_3$ NS [**40**], after the Gd^{+3} ions doping, insertion of the ions imparted a greater number of electrons in the crystal lattice. The undoped titanate NS showed absorptivity maximum (λ_{max}) 320 nm whereas 50 wt. % $GdTiO_3$ NS exhibited (λ_{max}) 650 nm. UV-Visible absorptivity values of the undoped titanate and 50 wt. % $GdTiO_3$ NS summarized in **Table 2**. Formation of polarized surface area due to well dispersion of Gd^{+3} ions into the titanate NS which intern facilitated the transfer of the electrons from the titanate layer [**41,42**]. Band-gap energies of the sample were calculated using Kubelka-Munk method. Kubelka-Munk factor was determined from the equation $K= (1-R)^2/2R$, where, R is the percentage of reflectance and intersection of the curves, the slope was evaluated to obtain the energy gap (Eg) of the NS (Tauc plot). For 50 wt. % of $GdTiO_3$ energy gap was found to be 2.89 eV.

Table 2. Comparison of optical absorptivity values of the undoped titanate and 50 wt. % of $GdTiO_3$ NS.

Nanostructures	Absorptivity	λ_{Min}	λ_{Max}	Absorption Region	Spectral range
Undoped Titanate	210 nm[a] 250 nm 280 nm 320 nm	210 nm	320 nm	Ultraviolet	210 -320 nm
50 wt. % $GdTiO_3$	310 nm[b] 350 nm 600 nm 650 nm	310 nm	650 nm	Ultraviolet-Visible	310-650 nm

[a,b](absorption minimum in UV- Visible spectrophotometer).

Impedance and current-voltage properties of pelletized $GdTiO_3$ NS

Impedance-Voltage characteristics of $GdTiO_3$ NS

The Current-voltage, capacitance-voltage and linearity curves for the pelletized samples of $GdTiO_3$ showed variable properties. **Fig. 5** display the nonlinear variation of impedance with the applied voltage. Applied voltage varied in between – 6V to + 6V, Impedance characteristics especially, variation in the resistance of the pelletized samples of 50 wt. % $GdTiO_3$ NS were experimentally determined by using Agilent 4294 model Keithley instrument and the values are summarized in **Table 3**. Highest resistance observed was 76555.2 Ω with a corresponding applied voltage of 6V as shown in **Fig. 5** Current gain was found to be 1.12×10^{-5} A at this junction of an applied voltage. The variation in impedance depends on the thickness of the pellet as well as the change in the morphology of the crystal upon making pellets [**43,44**]. Resistance value decreases at 1V with 29213 Ω and conductance of 3.423 × 10^{-5} S/m was observed. This increase in conductivity at a lower voltage is because the charge carrier density of Gd^{+3} ions increases on the surface of NS which intern increases the overall conductance of the $GdTiO_3$ NS. A decrease in conductivity at higher voltage is ascribed to the fact that interaction of Gd^{+3} ions in the crystalline phase restricts the mobility of the charge carrier in the heavily doped NS.

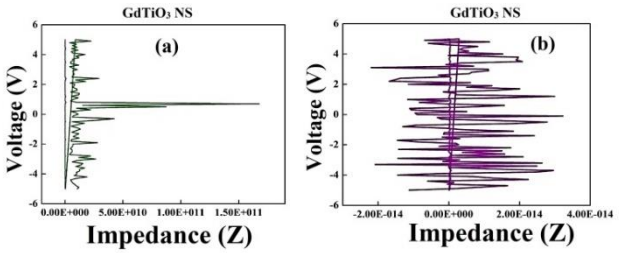

Fig. 5. (a) Impedance spectra of the pelletized samples of 50 wt. % $GdTiO_3$ at 500 KHz; (b) 1MHz respectively.

Table 3. Comparison of current gain, resistance and conductance of 50 wt. % pelletized samples of $GdTiO_3$ NS.

Samples	Voltage (V)	Current (A)	Resistance (Ω)	Conductance (S/m) × 10^{-5}
50 wt. % $GdTiO_3$	1	1.71×10^{-6}	29213	3.423[a]
	2.5	7.33×10^{-6}	38215.2	2.61
	4	9.99×10^{-5}	75042.7	1.33
	6	1.12×10^{-5}	76552.2	1.30

[a](observed highest power dissipation value); [b](Highest observed admittance).

Table 4. Impedance, admittance and power dissipation values of 50 wt. % $GdTiO_3$ NS.

Samples	Impedance (S) × 10^4	Admittance (S/m) × 10^{-5}	Power Dissipation (W)
50 wt. % $GdTiO_3$	2.92	3.42[b]	8.56×10^{-8}
	3.82	2.62	2.05×10^{-6}
	7.50	1.33	7.50×10^{-6}
	7.66	1.31	9.66×10^{-6}[a]

[a]Observed highest power dissipation value;
[b]Highest observed admittance.

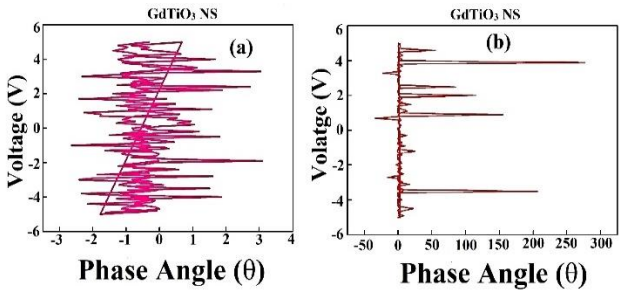

Fig. 6. (a) Variation in the phase angle theta with the applied voltage for 50 wt. % $GdTiO_3$ at 500 KHz; (b) variation in the phase angle theta for 50 wt. % $GdTiO_3$ at 1MHz.

Applied voltage and frequency angle (θ) characteristics of $GdTiO_3$ NS

The Average thickness (~ 200 µm to 400 µm) of the pelletized sample of $GdTiO_3$ NS subjected for recording variation in the current gain with frequency phase angle (θ) in between - 50 to 300 and applied voltage varied similarly from – 6V to +6V as shown in **Fig. 6**. Impedance, admittance, power dissipation values summarized in **Table 4**. Highest value of admittance and power dissipation offered by the pelletized sample of $GdTiO_3$ was 3.42 × 10^{-5} S/m and 9.66 ×10^{-6} W respectively. Power dissipation of the 50 wt. % $GdTiO_3$ NS varies from 9.66 × 10^{-6} W to 8.56 × 10^{-8} W with the value of impedance fluctuating in between 7.66 × 10^4 S to 2.92 ×10^4 S. Leakage current decreases as impedance and power dissipation value decreases which were found in the literature of Gd doped NS [**45,46**]. However, there is a gradual decrease in the admittance and impedance values as the applied frequency increases above 1MHz. It can be interpreted at low frequencies NS can harvest electrical signals which depend on the current gain. $GdTiO_3$ NS facile migration of the charged Gd^{+3} ions into the titanate surface resulted in low resistive areas. At higher frequencies stack of the interface of Gd^{+3} ions for

electrical signals occurred due to more resistance offered by the $GdTiO_3$ NS causing increases in power dissipation values. In this situation, the amount of conductance and power dissipation from the pelletized sample of $GdTiO_3$ NS interface state plays a vital role.

Conclusion

The present work describes different wt. % of $GdTiO_3$ NS synthesized by microwave-assisted synthesis followed by reduction using hydrazine hydrate. SEM analysis showed the morphology and average grain size, an interpore distance of the $GdTiO_3$ NS and was found to be ~ 62 nm and ~ 101 nm respectively. XRD studies revealed change in the crystal structures from the tetragonal geometry to agglomerated densely packed tetragonal structure with decrease in crystallite size as concentration of Gd^{+3} increases over titanate NS. XRD analysis indicates that NPs of Gd_2O_3/Gd^{+3} well incorporated into the titanate NS. The uv-visible spectroscopic investigation displayed a blue shift in the absorptivity of the NS doped with Gd^{+3} ions. Undoped titanate and 50 wt. % $GdTiO_3$ exhibited their absorptivity at 320 nm and 650 nm respectively. Increase in oxidation potential of the NS is observed due to surface polarization phenomena as the impurity percentage of Gd^{+3} upon 50 wt.% over titanate NS. Nonlinear Impedance values indicate that properties strongly dependent on the bias voltage and applied frequency. Bulk grain and grain-boundary contributions to the electrical resistivity and capacitance were studied through impedance analysis with a parallel resistance (R) and capacitance (C) circuit. The analysis confirms that impedance properties improve with Gd substitution into titanate NS. The C-V, impedance analysis and I-V characteristics infer that 50 wt. % doped $GdTiO_3$ NS strongly ohmic in nature. The impedance properties improve with Gd insertion and recorded highest conductance and power dissipation values of 3.42×10^{-5} S/m and 9.66×10^{-6} W respectively. The present investigation on current-voltage and impedance spectroscopic techniques are more innovative compared to other characteristics and find enormous application in device fabrication and further usage in the field of gas sensors, biosensors and light-harvesting devices.

Acknowledgements

Authors are thankful to MSRIT, Bangalore, India for spectroscopic characterization, CENSE, IISc, Bangalore, Karnataka, India for I-V, C-V and related experimentation to carry out.

Conflicts of interest

All the authors declare that they do not have any conflict of interest.

Keywords

$GdTiO_3$, Electrical Properties, Impedance, Power dissipation, Current-Voltage, Nanostructures.

Received: 13 December 2020
Revised: 13 January 2021
Accepted: 15 January 2021

References

1. Gao, L.; Dai, Y.; Li, T.; Tang, Z.; Zhao, X.; Li, Z.; Meng, X.; He, Z.; Li, J.; Cai, M.; Wang, X.; Zhu, J.; Xing, H.; Ye, W.; *J. Nanomater*., **2018**, *8*, 911.
2. Wei, L.; Ling, X.; Wei-Ming, Z.; Hong-LinD.; Zhong-Yuan, M.; Jun, X.; Kun-Ji, C.; *Chin. Phys. B.*, **2010**, *19*, 4.
3. Li, L.; Liang, J.; Chou, S.; *Sci. Rep*., **2015**, *4*, 4307.
4. Jiawei, J.; Zhang, Y.; Guochen, L.; Zengyong, C.; Gongyi, L.; *Mater. Chem. Phys.*, **2020**, *249*, 23016.
5. Ansari, Z. A.; Khalid, S.; Khan, A. A.; Fouad, H.; Ansari, S. G.; *Sensor Lett.* **2014**, *12*, 1495.
6. Suryakanta, N.; Banalata, S.; Tapan Kumar, C.; Dipak, K.; *RSC Adv.*, **2014**, *4*, 1212.
7. Yang Y.; Zhan-Sheng, G.; Minhao, Y.; Ming-Sheng Z.; Dong-Rui, W.; Jun-Wei, Z.; Yong-Qiang, W.; Zhi-Min, D.; *Nano Energy*, **2019**, *59*, 363.
8. Ravichandran, R.; Mani, D.; Marimuthu, G.; Naiyf, S. A.; Shine K.; Jamal, M. K.; Mohammed, N. A.; Roman, P.; Baskaralingam,V.; *J. Photochem. Photobiol. B.*, **2019**, *199*, 111620.
9. Meghmala S. W.; Aparna B. G.; Javed A. M.; Neha N. P.; Neelu N. N.; *SN Applied Sciences*, **2019**, *1*, 310.
10. Fu, L; Liu, Z; Liu, Y.; *Adv. Mater. Proc.*, **2004**, *16*, 350.
11. Burn, I; Neirman, S.; *J. Mater. Sci.*, **1982**, *17*, 3510.
12. Hwang, D. W; Lee, J. S; Li, W; Oh, S.H.; *J. Phys. Chem. B.*, **2003**, *107*, 4963.
13. Subramanian, M.A.; Aravamudan, G.; Subba Rao, G.V.; *Prog. Solid State Ch.*, **1983**, *15*, 55.
14. Zhou, W.Y.; Cao, Q.Y.; Liu, Y.J.; Yu, X.Y.; Luo, Y.; *Adv. Appl. Ceram*., **2007**, *106*, 222.
15. N. Yalini, D.; Vijayakumar, K.; Rajasekaran, P.; A.S. Alagar N.; Sidharth, D.; Shimomura, M.; Arivanandhan, M.; Jayavela, R. *Ceram. Int*., **2020**.
16. Rahmana M. T.; Ramana C. V.; *J. Appl. Phys.*, **2014**, *116*, 164108.
17. Bharathi, K.K; Garimella, M.; Ramana, C.V.; *J. Electrochem. Soc.* **2011**, *158*, G71.
18. Kuldeep, C, V.; Kotnala R. K.; Vivek, V.; Negi, N. S.; *Thin Solid Films*. **2010**, *518*, 3320.
19. Bonanos, N.; Pissis, P.; Macdonald, J.R.; E.N. Kaufmann (Ed.). **2012**.
20. Alexe-Ionescu, A. L.; Barbero, G.; Evangelista, L. R.; Lenzi, E. K.; *J. Phys. Chem. C.*, **2020**, *124*, 3150.
21. Filippo, G.; Antonio D. B.; Nadia, M.; Francesco, R.; Laura, I.; Paola, R.; Maurizio, P.; *Nanomaterials*, **2016**, *6*, 206.
22. Richard, G.; Yong, S.; Zhongjing R.; Liang, Z.; Hao, S.; Xiaoyu, S.; Jianping Y.; *J. Nanomater.*, **2017**, 8275139.
23. Liu, R. Cuiyun, J.; Fengjuan, S.; Jing, L.; *J. Nanomedicine.*, **2013**, *8*, 33-38.
24. Salaoru, I.; Paul S.; *Phil. Trans. R. Soc. A.*, **2009**, *367*, 4227.
25. Peter, M.; Minghu, Pan.; Pu, Y.; Ramamoorthy, R.; Arthur, P. B.; Sergei, V. K.; *Nanotechnology*, **2011**, *22*, 25.
26. Kamlesh V.; Chandekar, T.; Alshahrani, A.; Ben Gouider Trabelsi, F.H.; Alkallas, M.; AlFaify S.; *J. Mater. Sci.* **2020**, *56*, 4763.
27. Anurag, S.; Rajneesh, C.; Kirankumar, H.; Ambesh, D.; *J. Sol. Energy*, **2018**, *163*, 338.
28. Ganapathi Rao, G.; Lakshmi R. B.; Nirupama, V. *Mater. Chem. Phys*,.**2019**, *230*, 331.
29. Kasian, P.; Thongbai, P.; Yamwong, T.; Rujirawat, S.; Yimnirun, R.; Maensiri, S.; *J. Nanosci. Nanotechnol.*, **2015**, *15*, 9197.
30. Rahmana M.T.; Ramana, C.V.; *J. Appl. Phys.*, **2014**, *116*, 164108.
31. Mohd, S.; Aslam, K.; Hamdy, M.S.; AlFaify, S. *Mater. Res. Express*., **2020**, *6*, 1250.
32. Xu, G.B.; Yang, L. W.; Wei, X. L.; Ding, J, W.; Zhong, J. X.; Chu, P. K.; *J. Power Sources.*, **2015**, *295*, 305.
33. Manonmani, M.; Senthil, V. P.; Gajendiran, J.; *J. Mater. Sci. Mater. Electron.*, **2019**, *30*, 10934.
34. Hemasundara, R. S.; Muni Sudhakar, B.; Sudhakar, R. B.; Dhoble, S. J.; Thyagarajan, K.; Nageswara, R. C.; *J. Lumin.*, **2014**, *29*, 861.
35. Park, Y., Cho, K.; Kim, H.G.; *J. Am. Ceram. Soc.* **1998**, *81*, 1893.
36. Zhanshen, Z.; Wenshuo, K.; Yuanliang, L.; Rujie, Z.; Wenxin, D.; Yufan, W.; *J. Mater. Sci.: Mater. Electron.*, **2019**, *30*, 2743.
37. Yingying, Z.; Qinlong, W.; Zhaowen, R.; Hui, X.; Shiping, T.; Wancheng, Z.; *J. Alloy Compd.*, **2018**, *733*, 33.

38. Wenshuo, K.; Zhanshen, Z.; Yuanliang, L.; Rujie, Z.; Wenxin, D.; Yufan, W.; *J. Mater. Sci.: Mater. Electron.*, **2019**, *30*, 2743.
39. F.J.J. van Loo, J.J.J.; B. Pieraggi, B.; R.A. Rapp, R.A.; *Acta Mater.*, **1990**, *38*, 1769.
40. Xiaoli, X.; Lingbo, X.; Yanmin, J.; Zheng, W.; Feifei, W.; Yaojin, W.; Neale, O. H.; Haitao, H.; *Energy Environ. Sci.*, **2018**, *11*, 2198.
41. Dingze, L.; Pengfei, F.; Yang, L.; Zhi, L.; Xinzhao, L.; Yuanpeng, G.; Feitai, C.; Fei, N.; *J. Nanopart Res.*, **2014**, *16*, 2636.
42. Liang, S.; Lixin, C.; Rongjie, G.; Yanling, Z.; Huibin, Z.; Chenghui, X.; *J. Alloy. Compd.* **2014**, *617*, 756.
43. Tennery, V.J.; Cook, R.L.; *J. Am. Ceram. Soc.*, **1961**, *44*, 187.
44. Vojnovich, T.; Mcgee, T.D.; *J. Am. Ceram. Soc.* **1969**, *52*, 386.
45. Wei, W.; Xiaoguang, L.; Wanli, L.; Han, Z.; Jun, H.; Haicheng, W.; Yanglong, H.; *ACS Appl. Mater. Interfaces*, **2019**, *11*, 12752.
46. Panigrahi, S.C.; Piyush, R.D.; Parida, B.N.; Padhee, R.; Choudharya R.N.P.; *J. Alloy Compd.* **2014**, *604*, 73.

Authors biography

Prof. Dr. Vinayak Adimule has Thirteen years of research experience as Senior Scientist and Associate Research Scientist in R&D organisations of TATA (Advinus), Astra Zeneca India, Trans Chem Ltd. Expert in the area of Medicinal Chemistry (Anticancer Drugs), Nano science and Technology, Material Chemistry and Bio Chemistry. Published more than 30 research articles and book chapters in Scopus, Google Scholar (SJR) indexed journals, Attended and presented papers in National and International Conferences, Received Best Oral/Poster awards, published few books in Notion Press International Inc., Chaired few international and National Conferences, symposia related to Material Electronics. Editorial Board Member, Life Member and Associate Member for many international societies and research institutions. Recognised Research Guide VTU, Belagavi. Presently guiding one research scholar for PhD. Research interest includes Nano Electronics, Material Chemistry, Sensors and Actuators, Bio Nanomaterials, Medicinal Chemistry.

Dr. Debdas Bhowmik has 15 years of R&D Experimnce, published 30 International papers, delivered key note talks, attended many international and national workshops, conferences, symposium in the filed of propullants, medicinal chemistry, nanoscience and technology. Presently sir hold scientist F position in the DRDO (High Energy Materials Laboratory).

Adarsha Harmballi Jagadeesha working as research scholar in the area of medicianl chemistry, electrochemical devices, nanoscience and nanotechnology, presently in National University of Ireland, Mr. Adarsha HJ become the member for several socitirs like royal society of chemistry, ACS etc. also published several national and international papers in reputed journals.